Modeling Respiratory Lung Motion – a Biophysical Approach using Finite Element Methods

Rene Werner[a,b], Jan Ehrhardt[a], Rainer Schmidt[b], and Heinz Handels[a]

[a]Department of Medical Informatics, University Medical Center Hamburg-Eppendorf, Hamburg, Germany

[b]Department of Radiotherapy and Radio-Oncology, University Medical Center Hamburg-Eppendorf, Hamburg, Germany

ABSTRACT

Respiratory dynamics poses a main source of error in radiotherapy of thoracic tumors. Development and optimization of methods to adequately account for breathing motion require detailed knowledge of the dynamics and its impact on e. g. the dose delivered by radiation. Thus, computer aided modeling and model based simulation of respiratory motion gains in importance.

In this paper a biophysical approach for modeling lung motion is described. Main aspects of the process of lung ventilation are identified and outlined as the starting point of modeling. They are formulated as a contact problem of linear elasticity theory. The resulting boundary value problem is solved using Finite Element Methods (FEM). 4D (= 3D+t) CT image data are used to evaluate the modeling approach. Model based three-dimensional vector fields representing respiratory motion are computed for different patients. Simulated motion patterns of inner lung landmarks like prominent bifurcations of the bronchial tree and the tumor mass center are compared with corresponding motion patterns observed in the 4D CT data. The influence of geometrical and biomechanical parameters like mesh quality and values of elasticity constants on the modeling process is investigated.

Differences between model based predicted landmark positions and corresponding landmark positions identified interactively are mostly within the variability of interactive landmark positioning across multiple observers (interobserver variability). The impact of geometrical and biomechanical parameters on resulting vector fields is fairly small. Outcomes suggest that FEM state an adequate strategy to model aspects of the physiology of breathing.

Keywords: Biophysical modeling, FEM, Respiratory motion, 4D CT, Radiation therapy

1. INTRODUCTION

Radiation therapy aims at high tumor control and low normal tissue complication probabilities. Therefore the dose distribution should be focused on tumorous tissue, avoiding especially organs at risk. In current clinical practice identifying tissue to be irradiated and organs at risk is mostly based on three-dimensional (3D) imaging (in general computed tomography (CT)). But 3D imaging provides only for a static snapshot of the patient's anatomy. Consequently radiation therapy suffers from missing information regarding organ and tumor mobility. To ensure an adequate dose distribution within the moving tumor usually the volume to be irradiated is expanded.[1] This also increases the volume of irradiated healthy tissue and the likelihood of treatment-related complications becomes larger. This in turn limits attempts to escalate the dose delivered to the tumor in order to increase tumor control.

The problem becomes especially challenging in radiation therapy of thoracic tumors: Due to respiration lung tumors and organs at risk undergo motion of the magnitude of several centimeters.[2,3] Recently a variety of techniques to explicitly account for respiratory dynamics has been proposed (breath-hold techniques, respiratory gating, real-time tumor tracking). But, implementation and optimization of such techniques require detailed

---

Further author information: (Send correspondence to R.W.)
R.W.: E-mail: r.werner@uke.uni-hamburg.de, Telephone: +49 (40) 42803 2938

knowledge about respiratory dynamics and its impact on the dose delivered by radiation and resulting thoracic dose distributions.

Consequently, computer aided modeling and model based simulation of respiratory motion gains in importance: It helps to get a deeper understanding of the respiratory motion inside the human body; and in addition resulting simulations can be applied to problems of direct clinical relevance, e. g. dose accumulation.[4] Different approaches are proposed in the literature. Often non-linear registration methods are applied to images acquired at different breathing phases to estimate respiratory motion fields.[3, 5–7] In this case, underlying assumptions usually concern image-related aspects; physiological and anatomical processes are not taken into consideration. As an example in Ehrhardt et al.[3] and Handels et al.[7] we presented a non-linear registration method based on the optical flow constraint equation, that is, gray values of anatomically corresponding voxels are assumed to be constant over time. In this study we aim at modeling respiratory motion taking the physiology of breathing as modeling starting point. As an approved method in biophysical modeling we therefore apply Finite Element Methods (FEM). Previously e. g. Sundaram et al.[8] proposed an approach to modeling lung motion by means of FEM. They suggest an FEM-based registration approach assuming occurring deformations to be linear-elastic and taking into account normalized cross-correlation as similarity measure of fixed and deformed image. An other FEM-related approach is given by Santhanam et al.[9] accounting for PV relations in the lungs and limiting motion by direction constants. The reference to the physiology of breathing does not seem to be immediately apparent for these approaches. In comparison, DeCarlo et al.[10] proposed an approach which suggest itself: Using a two compartment model they try to simulate the process of lung ventilation by applying pressure forces to the surfaces of the lungs and the chest wall. Penetration of lung and chest wall cavity is avoided by collision detection. In the pilot study they used a simplified lung model which is defined in 2D; the shape is loosely based on the lung shape in a coronal view. A similar approach, but extended to 3D, is presented by Zhang et al.:[11] Lung ventilation is also modeled by applying pressure forces to the lung surfaces; lung expansion is limited by a second geometry representing the chest wall cavity. The implementation is based on contact elements of the FEM software ANSYS (ANSYS Inc., Canonsburg); no further implementation details on the contact elements are presented. The feasibility of the approach is shown by means of 3D lung models extracted from a breath-hold CT at end-expiration and at deep-inspiration.

Inspired by the work of Zhang et al.[11] we aim to refine their modeling approach. In this study we describe in detail the modeling approach and its reference to the physiology of breathing. In addition to Zhang et al. we deduce the corresponding contact problem of linear elasticity. The problem is solved by means of an augmented Lagrangian algorithm using the FEM software COMSOL Multiphysics (COMSOL AB, Sweden). There is no consensus in the values of lung tissue elasticity constants. For instance, Zhang et al.[11] chose Young's modulus E to be 4 kPa and Poisson's ratio $\nu = 0.35$, whereas Sundaram et al.[8] chose $E = 0.1$ kPa and $\nu = 0.2$. Therefore we analyze the impact of different values of elasticity constants (biomechanical parameters) on the modeling process. The impact of geometrical parameters (mesh quality) is considered as well. Previous literature especially suffers from missing evaluation data. For instance, DeCarlo et al.,[10] Zhang et al.,[11] and Santhanam et al.[9] presented no quantitative evaluation data. Sundaram et al.[8] only used 2D MR images with low spatial resolution. Recently the development of 4D imaging opened up the possibility to measure motion of inner organs and tumors and, consequently, to verify modeling approaches. In this study we use 4D (= 3D+t) CT image data with high spatial and temporal resolution for the evaluation of modeling accuracy. For evaluation purposes we compare model based predicted positions of inner lung landmarks and corresponding landmark positions identified interactively.

2. METHODS AND MATERIALS

4D data sets open up the possibility to measure breathing motion of inner organs (e. g. the lungs) and tumors. Depending on image quality and resolution, they enable the verification of respiratory motion modeling approaches. In this study we use spatially and temporally high resolved 4D CT image data of lung tumor patients. Patients were examined with a 16-slice CT scanner (Brilliance, Philips Medical Systems, Cleveland) in cine mode. For each patient between 15 to 25 scans per couch position were acquired continuously (gantry rotation time: 0.5 s, dead time between scans: 0.25 s). In-plane resolution was between 0.94×0.94 and 0.98×0.98 mm², slice thickness was 1.5 mm. For further data acquisition details see Low et al.[12] and Lu et al.[13] The resulting spatiotemporal series of CT scans (each scan covering only a part of the thorax for a given breathing phase!) were

2

used to reconstruct 4D CT data sets representing a series of 3D CT images (each covering the whole thorax) for a scale of user-defined breathing phases. We chose the temporal resolution to be 10 to 14 breathing phases sampled equidistantly over the breathing cycle. Reconstruction was accomplished by an optical flow based reconstruction method.[14–16] In contrast to other reconstruction methods[12] motion artifacts are reduced significantly; hence the image data provide a solid foundation for motion analysis and model verification. In this study four patient data sets with different breathing-related motion amplitudes and tumor locations are considered for evaluation purposes.

2.1 Modeling approach

Starting point of modeling is the process of lung ventilation. The lungs themselves are not actively moving. Each lung is located in the pleural sac build up by two membranes called the pleurae. Outer pleura (parietal pleura) is adherent to the internal surface of the thoracic cavity and the diaphragm. Inner pleura (visceral pleura) covers the lung and is adherent to its surface. Parietal and visceral pleura are joined together at the root of the lung. The space enclosed is known as the pleural cavity. It is subject to a negative pressure (the intrapleural pressure) and filled with a fluid. Due to the negative pressure the pleurae are in close contact. The contact is frictionless due to the fluid within the pleural cavity. During breathing the thoracic cavity is expanded by contraction of the diaphragm and outer intercostal muscles. This causes changes in the intrapleural pressure which acts as a force upon the lung surface. Hence lung expands, and during this process the visceral pleura is sliding frictionlessly down the internal surface of the thoracic cavity.

This process is modeled as a contact problem of elasticity theory. A uniform negative pressure (intrapleural pressure) is applied to a lung surface (except for the region of the root of the lung, which is assumed to be fixed) representing some initial state of breathing; we choose the initial state of breathing to be the state of end-expiration (EE). The pressure magnitude is increased gradually starting with a zero pressure. Increasing the pressure causes the lung to expand whereas expansion is limited by a geometry representing the lung shape at a final state of breathing; we choose the final state to be end-inhalation (EI). Principle and terminology are illustrated in fig. 1. We aim for a state in which the initial lung geometry deformed by the intrapleural pressure nearly matches the limiting geometry. This state should be an equilibrium state, i. e. external forces should be balanced out by inner lung reacting forces specified by the Cauchy stress tensor σ. Given equilibrium the corresponding deformation field $\mathbf{u} : \mathbb{R}^3 \rightarrow \mathbb{R}^3$ is searched for. $\mathbf{u}$ is interpreted to be an estimation of the inner lung motion field during breathing (here: from EE to EI). As no volume forces are modeled equilibrium is characterized by:

$$\operatorname{div} \sigma = 0 \tag{1}$$

Lung tissue is assumed to be an isotropic linear elastic and homogeneous medium; hence the constitutive equation is given by generalized Hooke's law:

$$\mathbf{S} = \mathbf{C}\left(E, \nu\right) \varepsilon \tag{2}$$

whereas

$$\varepsilon = \frac{1}{2}\left(\nabla \mathbf{u} + \nabla \mathbf{u}^T + \nabla \mathbf{u}^T \nabla \mathbf{u}\right) \tag{3}$$

represents the Green-Lagrange strain tensor, $\mathbf{S}$ denotes the 2nd Piola-Kirchhoff stress tensor, and $\mathbf{C}\left(E, \nu\right)$ is the elasticity tensor which depends on two elastic constants (we choose E: Young's modulus and ν: Poisson's ratio). Lung volume changes are in the order of $20\,\%$ of the lung volume at EE within a breathing cycle, i. e. large deformations are expected to occur; therefore Green-Lagrange strain tensor is used which enables for large deformation analysis. Green-Lagrange strains and 2nd Piola-Kirchhoff stresses are defined with reference to the undeformed state (initial state). They are linked to the the deformed state by $\sigma = (1/\det \mathbf{F})\, \mathbf{F}\, \mathbf{S}\, \mathbf{F}^T$ whereas $\mathbf{F} = \nabla \mathbf{u} + \mathbf{I}$ represents the deformation gradient. Equations 1 to 3 form the governing equations of the problem to be solved. The problem specification is completed by the boundary conditions: No displacements are allowed at the root of the lung, and the limiting geometry is also fixed:

$$\mathbf{u} = \mathbf{0} \quad \text{for the root of the lung and the limiting geometry} \tag{4}$$

No penetration of deformed initial lung geometry and limiting geometry should occur. This states a contact problem (here: frictionless contact) which yields additional boundary conditions to be fulfilled on the deformed initial
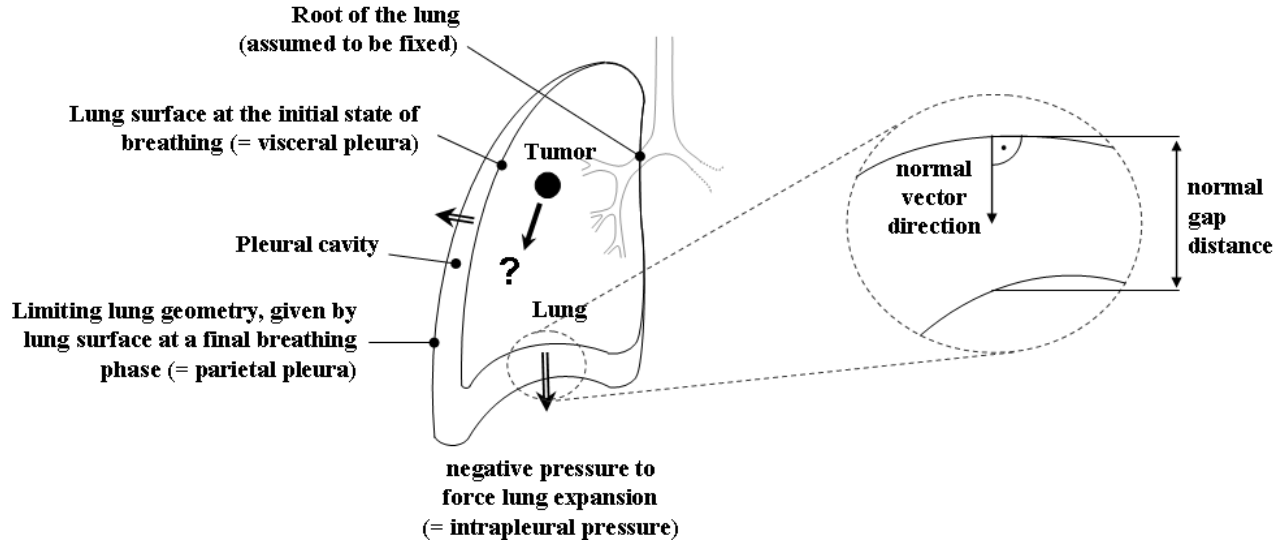
3

Figure 1. For illustration of the modeling approach and the terminology used. The normal gap distance specifies the distance between deformed initial lung surface and limiting geometry surface; it is determined by orthogonal projection. Note that normal vector points outwards from the deformed initial lung surface.

geometry surface. These boundary conditions are known as *Signorini conditions*:[17] In case of contact between deformed initial lung geometry surface and limiting geometry surface penetration is prevented by introducing compressive contact forces:

$$g \geq 0 \tag{5}$$

$$p_{\text{contact}} \leq 0 \tag{6}$$

$$p_{\text{contact}} \cdot g = 0 \tag{7}$$

whereas g denotes the normal gap distance, i. e. the distance between the deformed initial geometry surface and the limiting geometry surface ($g > 0$: separation, $g = 0$: contact, $g < 0$: penetration), and $p_{\text{contact}}\mathbf{n}$ are the contact forces with $\mathbf{n}$ the normal vector pointing outwards the deformed lung surface (see fig. 1). Contact pressure and intrapleural pressure together define the stress boundary conditions:

$$\sigma\mathbf{n} = (p_{\text{intrapl}} + p_{\text{contact}})\,\mathbf{n} \tag{8}$$

($p_{\text{intrapl}} \geq 0$: intrapleural pressure). Equations 1 to 8 represent the boundary value problem to be considered.

2.2 Implementation and evaluation

Given the weak formulation of the boundary problem described, it can be solved using Finite Element Methods. In this study we used the FEM software COMSOL Multiphysics. The contact conditions stated by eq. 5 to 7 are satisfied using an augmented Lagrangian method, which means the system is solved in a segregated way: In a first step the problem is solved for the displacement variables keeping the contact pressure constant. After this the contact pressure is solved for while keeping the displacement variables fixed. These two steps are iterated until the contact conditions are satisfied for the prescribed intrapleural pressure. For further details regarding the augmented Lagrangian method see e. g. Bertsekas[18] or Zienkiewicz et al.[19]

In a first part of the study we investigate the influence of biomechanical and geometrical parameters on the modeling process. The impact of the elasticity modulus E and Poissons ratio ν upon the intrapleural pressure required to reach the state in which deformed initial geometry nearly matches the limiting geometry is analyzed. Success criterion is a ratio between the limiting lung geometry volume and the deformed initial lung geometry volume of more than 0.99; as no penetration is allowed the ratio is between 0.99 and 1.0 if the criterion is fulfilled.

4

According to parameter values proposed in previous literature[8,11] the values range from 0.25 to 1.0 kPa for the elasticity modulus and 0.1 to 0.4 for Poisson's ratio. Increasing elasticity modulus E and/or Poisson's ratio ν produces stiffer response to external forces; thus higher E and ν values should require higher pressures to reach the volume ratio aimed for. Given an isotropic linear elastic medium loaded uniformly the relationship between pressure change and volume change (subjected to E and ν) can be stated as:

$$dp\,(E, \nu) = -\frac{dV}{V_i} \cdot \frac{E}{3\,(1 - 2\nu)} \tag{9}$$

(dp: pressure change; dV: volume change; V_i: volume of the undeformed initial lung geometry). In the present case, the contact pressure acts only in case of contact; consequently the pressure applied is not uniformly in a strict sense. The question arises to what extent eq. 9 allows for an estimation of the pressure required to reach a volume ratio of 0.99; this is investigated. Furthermore, given convergence the influence of different values of E and ν on the displacement field $\mathbf{u}$ is analyzed. Therefore the initial, undeformed domain is discretized by voxelization (voxel dimensions $1 \times 1 \times 1$ mm) and corresponding displacement vectors computed are compared with each other for different E and ν values. The studies are executed at a "normal" mesh quality level. We use tetrahedrons as finite element type. Element quality is determined using an aspect ratio measure suggested by the COMSOL package:

$$q = 72 \cdot \sqrt{3} \cdot \frac{V}{\left(\sum_{i=1\ldots6} l_i^2\right)^{3/2}} \tag{10}$$

whereas V is the volume element and l_i are the tetrahedron edge lengths. The impact of decreasing meshing quality on the modeling results is analyzed as well. Again corresponding voxel displacement vectors are compared, now varying mesh element size while keeping elastic constants fixed (here: $E=500$ kPa, $\nu=0.3$). Increasing mesh element size means decreasing element quality. Mesh quality is defined by the minimal element quality. This first part of our study is carried out by means of a simplifying mathematical phantom of the lung geometry in the style described by Staniszewska:[20] the shape of the lung approximates to that of a quarter of an ellipsoid. The analytical description of the phantom shape enables for the use of the build-in CAD tool of the FEM Software; as well meshing is done by a build-in mesh generator. Mesh quality values considered vary between 0.21 ("extremely fine mesh") and 0.06 ("extra coarse mesh") whereas 0.17 is the mesh quality for a "normal mesh".

The second part of the study is to generate and evaluate patient specific models based on the 4D CT image data. Initial lung geometry and limiting geometry definitions are extracted from CT image data. This requires additional preprocessing steps: The lungs are segmented in the CT image data at EE and EI. Region growing techniques and morphological operators are applied for segmentation; if necessary, the segmented structures are corrected manually. Based on the segmented data, triangulated 3D surface models are generated using the Marching Cubes algorithm.[21] The Marching Cubes Algorithm applied to binary images yields so called 'staircase artifacts' and a large number of triangles. As forces are determined to be surface forces directed along the surface normals (see eq. 8) the modeling approach relies on realistic, smooth surfaces. Therefore the artifacts are reduced by smoothing the surface models using Laplacian smoothing. The large number of triangles affects computational costs; it is decreased by applying an edge collapsing algorithm. These preprocessing steps are executed using MeVisLab (MeVis Research GmbH, Bremen, Germany). The smoothed and decimated surface models are imported to the FEM software via STL files representing the geometry definitions. As before, we use tetrahedral elements for meshing. Parameter values (elasticity modulus, Poisson's ratio, final intrapleural pressure, mesh size) are chosen according to the results of the studies based on the mathematical phantom. Modeling accuracy is evaluated comparing simulated patient specific motion patterns of inner lung landmarks and corresponding motion patterns observed in the 4D CT data. Landmarks are identified in the CT image data at EE and EI by up to six medical experts. For each landmark the interobserver variability with respect to landmark localization is determined. Based on the landmark location at EE which is identified by a "median observer" (landmark position = median of x, y, and z coordinates with respect to the coordinates determined by the multiple observers) we predict the landmark position at EI by adding the corresponding displacement vector given by the computed displacement field $\mathbf{u}$. Differences between landmark positions at EI as observed by the median observer and corresponding positions predicted by the model are analyzed. Landmarks considered are mass centers of the lung tumors and prominent bifurcations of the bronchial tree, see fig. 2 and table 1.

① right lung apex
② left lung apex
③ first bifurcation of the right main bronchus
④ second bifurcation of the right main bronchus
⑤ first bifurcation of the right lower lobe bronchus
⑥ bifurcation of the left main bronchus
⑦ first bifurcation of the left upper lobe bronchus
⑧ first bifurcation of the left lower lobe bronchus
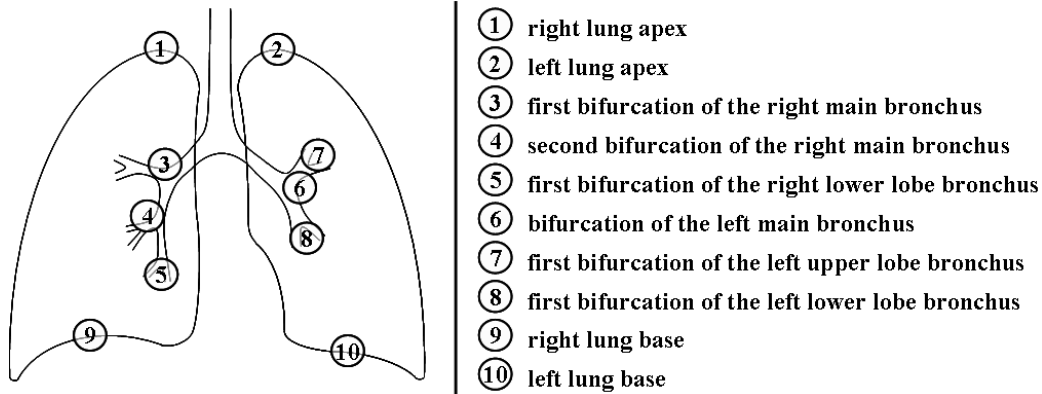⑨ right lung base
⑩ left lung base

Figure 2. Inner lung landmarks to be considered for modeling accuracy evaluation. Not included in this figure are the lung tumors mass centers. Tumors of the patients are located in the right upper lung lobe, the right lower lung lobe, the left upper lung lobe near the chest wall, and in the left lower lobe.

Table 1. Motion amplitudes of the inner lung landmarks as observed in the 4D CT data and averaged over the four patients (CC: craniocaudal; AP: anteroposterior; RL: lateral, right-left). Tumor mobility is evaluated by tracking the tumor mass center based on tumor segmentations.

	Motion amplitude (avg±std)			
Landmark	total	CC	AP	RL
right lung apex	3.2±1.9 mm	0.3±0.1 mm	3.0±1.7 mm	1.0±0.9 mm
left lung apex	4.2±2.3 mm	0.7±0.6 mm	3.1±1.5 mm	2.7±1.7 mm
first bifurcation of the right main bronchus	5.6±2.6 mm	5.2±1.8 mm	2.0±1.8 mm	1.1±0.5 mm
second bifurcation of the right main bronchus	7.5±3.5 mm	5.8±2.4 mm	4.8±2.6 mm	0.8±0.6 mm
first bifurcation of the right lower lobe bronchus	9.4±2.7 mm	8.6±1.5 mm	2.5±1.5 mm	2.6±1.6 mm
bifurcation of the left main bronchus	8.6±3.6 mm	7.9±2.8 mm	2.9±2.0 mm	2.2±1.3 mm
first bifurcation of the left upper lobe bronchus	6.8±3.0 mm	5.5±2.4 mm	3.2±1.5 mm	2.5±1.1 mm
first bifurcation of the left lower lobe bronchus	7.6±3.1 mm	6.8±2.5 mm	2.9±1.5 mm	1.9±1.1 mm
right lung base	12.7±6.1 mm	10.3±2.9 mm	6.3±5.1 mm	4.1±1.8 mm
left lung base	16.5±4.5 mm	14.1±3.1 mm	7.7±2.7 mm	3.5±1.7 mm
Patient 1: tumor in the right upper lobe	2.2 mm	0.8 mm	2.0 mm	0.1 mm
Patient 2: tumor in the right lower lobe	12.0 mm	11.4 mm	1.9 mm	1.1 mm
Patient 3: tumor in the left upper lobe	6.8 mm	2.9 mm	6.1 mm	0.7 mm
Patient 4: tumor in the left lower lobe	19.6 mm	19.5 mm	0.3 mm	1.0 mm

3. RESULTS

3.1 Influence of biomechanical and geometrical parameters on the modeling approach

As described in section 2.2 the intrapleural pressure needed to meet the success criterion (ratio between initial lung geometry volume and the limiting geometry volume of at least 0.99) depends on the values of the elasticity constants: The higher the values of E and ν, the higher the pressure required to deform the lung geometry. This is illustrated in fig. 3 by means of the mathematical phantom: the volume ratio is plotted against the intrapleural pressure applied for different values of the elasticity modulus E and Poisson's ratio ν. The figure shows, that eq. 9 is an underestimate of the pressure needed to reach a volume ratio of at least 0.99; a higher pressure is required. For further analyzes we considered the final pressure to be 2-times the pressure suggested by eq. 9 so the success criterion is fulfilled for all data sets (phantom-based as well as patient data sets).

Still considering the mathematical phantom, the influence of different E and ν values on the displacement field **u** can be shown to be fairly small: model based predicted voxel positions (= initial voxel position + corresponding
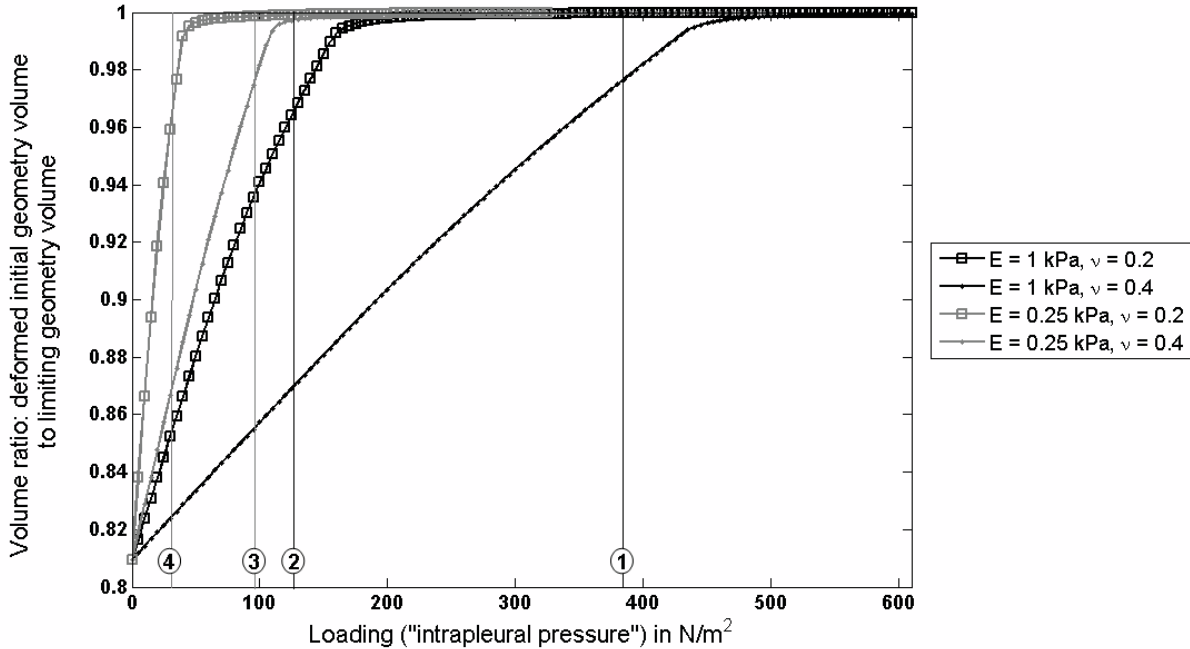
6

Figure 3. Ratio between the volume of the deformed initial lung geometry and the limiting geometry volume, plotted against the pressure applied (except for contact pressure, i. e. only the "intrapleural pressure" is shown here). The higher the values of the elasticity modulus E and Poisson's ratio ν, the higher the pressure needed to deform the lung geometry. Vertical lines indicate the pressure sufficient to overcome the volume difference between initial and limiting lung geometry according to eq. 9 (1: $E = 1$ kPa, $\nu = 0.4$; 2: $E = 1$ kPa, $\nu = 0.2$; 3: $E = 0.25$ kPa, $\nu = 0.4$; 4: $E = 0.25$ kPa, $\nu = 0.2$); as apparent underlying assumptions lead to an underestimation of the pressure required to fulfill the success criterion.

displacement vector) do not differ more than 0.5 mm for the E and ν values considered; no systematics can be found regarding the relationship between E and ν values and the differences. This also counts for different element sizes – given a minimum element quality of at least 0.17 ("normal" mesh quality level). Below this no closed contact between limiting geometry surface and deformed initial lung surface can be achieved. This means increased discretization errors (compared to discretization levels of "normal" or better) cause contact identification to fail. Because decreasing element size results in a greater number of degrees of freedom (dof) and higher computational costs ("normal" mesh quality: approx. 25.000 dof and 2 min for solving using a bi-processor system with Intel Xeon dual-core processors; "extremely fine: approx. 230.000 dof, solving needs more than five hours, same system), we use the "normal" mesh quality level for further study steps, i. e. for generating the patient specific models based on the 4D CT image data. It should be noted that the higher complexity of the patient specific lung geometries results in meshes consisting of a greater number of elements (approx. 40.000 to 70.000 dof). For the patient specific models solving times are approximately half an hour to one hour.

3.2 Evaluation of the modeling accuracy

Evaluating modeling accuracy is based on the patient specific models and the 4D CT image data as described in section 2.2. For illustration a patient specific lung geometry at the initial situation (at end-expiration) and the corresponding model based predicted lung shape at end-inspiration is shown in fig. 4. The gap distance is visualized for the initial and the final situation color-coded; it appears that for this patient the distance between initial and final lung surface is maximal in the region of the diaphragm due to a preponderance of abdominal breathing (in comparison to thoracic breathing). In fig. 5 corresponding motion field estimates (motion amplitudes) are visualized color-coded. Other distributions of the gap distance values and motion amplitude values are possible due to other breathing types.

For the patients considered it can be shown that differences between model based predicted motion patterns of inner lung landmarks and corresponding motion patterns observed by the median observer mostly are within
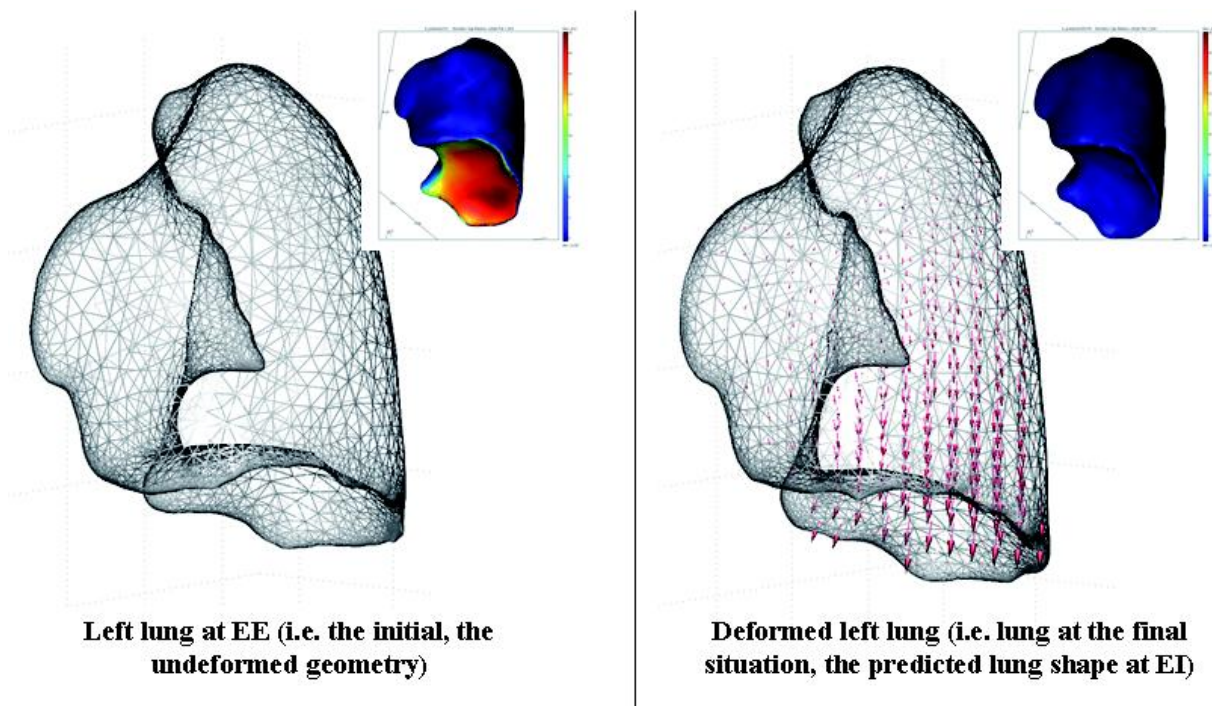
7

Figure 4. Left: the surface mesh of left lung at end expiration. Right: the surface mesh at simulated end inspiration. The arrows indicate the direction of motion; the arrow length is proportional to the motion amplitude. The small pictures in each right upper corner represent the distance between the surface of the lung to be deformed and the limiting geometry surface (red: distance of up to 20 mm; dark blue: no distance, i. e. contact is present).
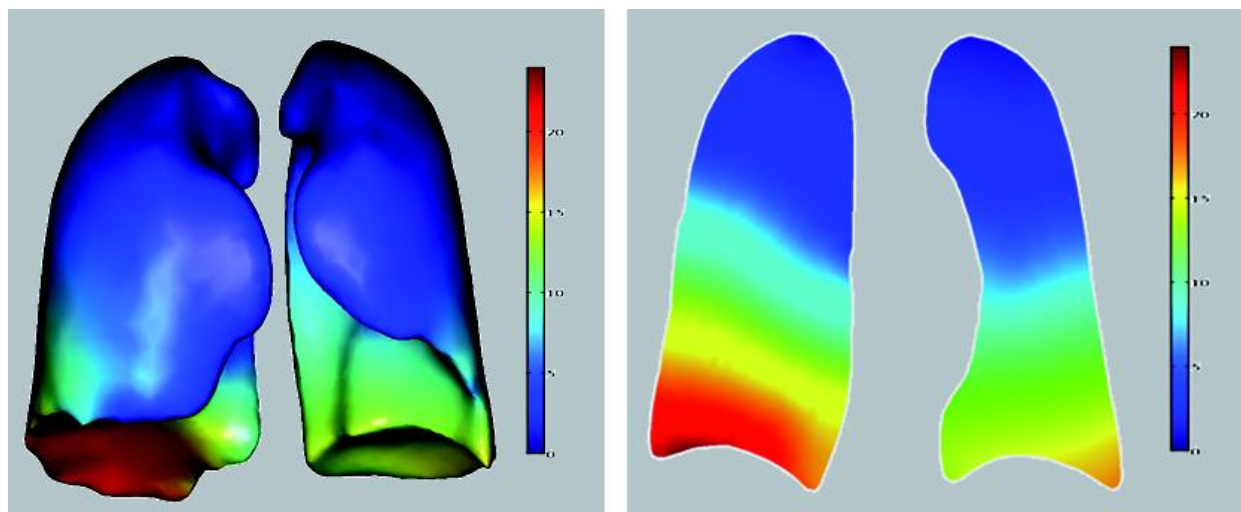

Figure 5. Color-coded visualization of computed displacement vector amplitudes (blue: small motion; red: motion of up to 24 mm). Left: motion of the lung surface. Right: inner lung motion, illustrated by means of a coronal slice.

the interobserver variability in landmark positioning as determined for the observers. For the tracheal bifurcations differences from 2 to 7 mm between predicted and observed landmark positions at EI are determined (mean value: 4.4±1.6 mm); interobserver variabilities are between 2 and 14 mm (mean value: 7.0±3.7 mm). Model based predicted and observed tumor positions at EI differ between 1.1 and 4.0 mm; no dependency between the

Table 2. Differences (averaged over the four patients) between the landmark localization at end inspiration as determined by model based prediction and the landmark position at EI as identified by a median observer (see text for definition).

Landmark	Difference between model based prediction and manual landmark localisation at EI (avg±std)			
	total	CC	AP	RL
right lung apex	2.7±1.3 mm	1.3±1.2 mm	1.9±1.5 mm	0.2±0.2 mm
left lung apex	2.5±1.2 mm	0.6±0.9 mm	2.1±1.4 mm	0.4±0.3 mm
first bifurcation of the right main bronchus	5.3±0.1 mm	3.4±2.0 mm	2.6±2.5 mm	0.4±0.3 mm
second bifurcation of the right main bronchus	7.4±3.5 mm	2.1±0.8 mm	6.3±4.5 mm	1.1±0.7 mm
first bifurcation of the right lower lobe bronchus	4.3±2.0 mm	1.6±1.3 mm	1.1±1.1 mm	3.1±2.5 mm
bifurcation of the left main bronchus	2.9±2.2 mm	2.2±1.8 mm	1.6±0.9 mm	0.9±0.4 mm
first bifurcation of the left upper lobe bronchus	4.3±2.0 mm	1.7±2.2 mm	3.2±1.4 mm	1.3±0.9 mm
first bifurcation of the left lower lobe bronchus	3.2±1.9 mm	2.0±1.3 mm	1.2±1.2 mm	1.8±1.5 mm
right lung base	5.3±2.0 mm	3.9±1.9 mm	1.7±1.4 mm	2.6±1.4 mm
left lung base	6.6±3.1 mm	3.0±2.0 mm	4.1±2.1 mm	2.3±3.8 mm
Patient 1: tumor in the right upper lobe	2.0 mm	0.4 mm	1.4 mm	1.4 mm
Patient 2: tumor in the right lower lobe	1.1 mm	0.9 mm	0.6 mm	0.1 mm
Patient 3: tumor in the left upper lobe	2.9 mm	2.9 mm	0.0 mm	0.2 mm
Patient 4: tumor in the left lower lobe	4.0 mm	4.0 mm	0.1 mm	0.8 mm

Table 3. Interobserver variability regarding manual landmark positioning, listed for the bronchial tree bifurcations (identification of the tumor mass centers based on tumor segmentations is only done once). Values are averaged over the patients data sets and the two breathing phases of end-expiration and end-inspiration.

Landmark	Interobserver variability regarding landmark positioning			
	total	CC	AP	RL
right lung apex	±3.0 mm	±1.3 mm	±2.1 mm	±1.7 mm
left lung apex	±4.8 mm	±1.4 mm	±3.7 mm	±2.6 mm
first bifurcation of the right main bronchus	±3.5 mm	±1.5 mm	±2.2 mm	±2.3 mm
second bifurcation of the right main bronchus	±9.0 mm	±5.5 mm	±6.4 mm	±3.2 mm
first bifurcation of the right lower lobe bronchus	±9.7 mm	±6.5 mm	±5.1 mm	±5.0 mm
bifurcation of the left main bronchus	±4.7 mm	±3.6 mm	±2.4 mm	±1.8 mm
first bifurcation of the left upper lobe bronchus	±7.5 mm	±4.3 mm	±3.8 mm	±4.9 mm
first bifurcation of the left lower lobe bronchus	±2.6 mm	±1.5 mm	±1.7 mm	±1.4 mm
right lung base	±11.0 mm	±6.2 mm	±8.1 mm	±4.1 mm
left lung base	±14.2 mm	±6.8 mm	±10.9 mm	±6.2 mm

differences and the tumor motion amplitude (2 to 20 mm, see table 1) can be identified. Differences between model based predicted and observed landmark location at EI are listed in table 2 for the different landmarks. Corresponding interobserver variabilities are given by table 3.

4. DISCUSSION

We presented a biophysical approach for modeling respiratory lung motion implemented by Finite Elements Methods. Using 4D CT data with high spatial and temporal resolution allows us for patient specific modeling and evaluating modeling accuracy. Outcomes show that the accuracy of model based prediction of landmark localization is comparable to manual landmark positioning: differences between model based predicted landmark positions and corresponding localizations determined by a median observer are mostly within the interobserver variability determined for the landmarks. Thus, Finite Element Methods state an adequate strategy to model aspects of the physiology of breathing – provided that such aspects can be formulated as a boundary problem. As denoted in the introduction there exist other approaches besides FEM for respiratory lung motion modeling.

9

For instance in Ehrhardt et al.[3] and Handels et al.[7] we presented an optical flow based non-linear registration. Discrepancies are apparent in motion patterns when comparing the approaches and corresponding motion field estimates respectively. The question arises what motion field tends to be more realistic. Moreover, are occurring differences of relevance with respect to issues of clinical importance like dose accumulation? These questions we will address in future research.

We assumed lung tissue to be isotropic linear elastic and homogeneous. This requires a dimensioning of the elastic constants (elastic modulus E, Poisson's ratio ν). By means of a mathematical phantom we investigated the impact of varying the values of the elastic constants on the modeling process. In previous literature a diversity of E and ν values of lung tissue are listed. We showed that varying the values influences the computed displacement fields (which are searched for) only very slightly. Thus, elastic constants dimensioning is of circumstantial relevance given the described approach. It should be noted that lung tissue in fact behaves visco-elastically (see e. g. Fung et al.[22]). Our assumption of lung tissue to be linear elastic is a simplifying assumption. This also counts for the assumption that lung tissue is homogeneous. The lung contains different structures like the bronchial tree, vessels and so forth. Therefore it is not a homogeneous medium. In future research we will drop these simplifying assumptions. This in turn might increase computational costs. Resulting motion field estimations will be compared to the simulations based on the simplified models. Will there be significant differences?

In this study we evaluated modeling accuracy by means of inner lung landmarks identified manually by multiple observers. Landmarks are identified in 4D CT data of high spatial resolution. Thus, the interobserver variability determined (up to 1 cm) seems to be quite large. In order to rate appropriateness of approaches for motion field estimation and especially to compare the different approaches the interobserver variability has to be reduced (e.g. by supporting the observer by partially automatizing the landmark positioning) or landmark positioning has to be automatized. Currently we are working on both these approaches.

ACKNOWLEDGMENTS

REFERENCES

1. International Commission on Radiation Units and Measurements (ICRU), *Prescribing , recording, and reporting photon beam therapy (supplement to ICRU report 50)*, Bethesda, Md., 1999 (IRCU report 62).
2. Langen, K.M., and Jones, D.T., "Organ motion and its management", Int J Radiat Oncol Biol Phys **50**, pp. 265–78, 2001.
3. Ehrhardt, J., Werner, R., Frenzel, T. et al.: "Analysis of Free Breathing Motion Using Artifact Reduced 4D CT Image Data", in *Medical Imaging: Image Processing*, Pluim, P.W., Reinhardt, J.M., eds., *Proc. SPIE* **6512**, pp. 1N1–11, 2007.
4. Keall, P.J., Mageras, G.s., Balter, J.M. et al., "The management of respiratory motion in radiation oncology report of AAPM Task Group 76", Med Phys **33**, pp. 3874–900, 2006.
5. Sarrut, D., Boldea, V., Ayadi, M. et al., "Nonrigid registration method to assess reproducibility of breath-holding with ABC in lung cancer", Int J Radiat Oncol Biol Phys **61**, pp. 594–607, 2004.
6. Boldea, V., Sarrut, D., Clippe, S. et al., "Lung Deformation Estimation with Non-rigid Registration for Radiotherapy Treatment", in Ellis, R.E., Peters, T.M., eds., *MICCAI 2003, Volume 2878*, pp. 770–7, 2003.
7. Handels, H., Werner, R. Schmidt, R. et al., "4D medical image computing and visualization of lung tumor mobility in spatio-temporal CT image data", Int J Med Inform **76S**, pp. S433-39, 2007.
8. Sundaram, T.A. and Gee, J.C. et al., "Towards a model of lung biomechanics: pulmonary kinematics via registration of serial lung images", Medical Image Analysis **9**, pp. 524–37, 2005.
9. Santhanam, A.P., Fidopiastis, C.M., Langen, K. et al., "Visualization of tumor-influenced 3D lung dynamics", in *Medical Imaging: Image Processing*, Reinhardt, J.M., Pluim, P.W., eds., *Proc. SPIE* **6144**, pp. 61410C-1–12, 2006.

10. DeCarlo, D., Kaye, J., Metaxas, D. et al., "Integrating Anatomy and Physiology for Behavior Modeling", in *Proc. 4th Conf. Medicine Meets Virtual Reality (MMVR IV)*, pp. 81–7, 1996.

11. Zhang, T., Orton, N.P., Mackie, T.R. et al., "Technical note: A novel boundary condition using contact elements for finite element based deformable image registration", Med Phys **31**, pp. 2412–5, 2004.

12. Low, D.A., Nystrom, M., Kalinin, E. et al., "A method for the reconstruction of four-dimensional synchronized CT scans acquired during free breathing", Med Phys **30**, pp. 1254–63, 2003.

13. Lu, W., Parikh, P.J., El Naqa, I.M. et al., "Quantitation of the reconstruction quality of a four-dimensional computed tomography process for lung cancer patients", Med Phys **32**, pp. 890–901, 2005.

14. Ehrhardt, J., Werner, R., Frenzel, T. et al., "Reconstruction of 4D–CT data sets acquired during free breathing for the analysis of respiratory motion", in *Medical Imaging: Image Processing*, Reinhardt, J.M., Pluim, P.W., eds., *Proc. SPIE* **6144**, pp. 2141–8, 2006.

15. Ehrhardt, J., Werner, R., Sring, D. et al., "An optical flow based method for improved reconstruction of 4D CT data sets acquired during free breathing", Med Phys **34**, pp. 711–21, 2007.

16. Werner, R., Ehrhardt, J., Frenzel, T. et al., "Motion artifact reducing reconstruction of 4D CT image data for the analysis of respiratory dynamics", Methods of Information in Medicine **46**, pp. 254–60, 2007.

17. Kikuchi, N., and Oden, J.T., *Contact problems in elasticity: a study of variational inequalities and finite element methods*, Philadelphia, SIAM, 1988.

18. Bertsekas, D.P., *Constrained Optimization and Lagrange Multiplier Methods*, Academic Press, New York, 1982.

19. Zienkiewicz, O. C., and Taylor, R. L., *The Finite Element Method for Solid and Structural Mechanics*, Elsevier Butterworth-Heinemann, 2005 (6th ed.).

20. Staniszewska, M.A., "A modification of Cristy's mathematical human phantoms for Monte Carlo simulation", J Radiol Prot **12**, pp. 85–92, 1992.

21. Lorensen, W.E., and Cline, H.E., "Marching cubes: A high resolution 3-D surface construction algorithm", Comput Graph **21**, pp. 163–9, 1987.

22. Fung, Y. C., *Biomechanics: Motion, Flow, Stress, and Growth*, Springer-Verlag, 1990.